IEEE Access
Multidisciplinary | Rapid Review | Open Access Journal

Received February 4, 2016, accepted March 4, 2016, date of publication April 20, 2016, date of current version June 13, 2016.

Digital Object Identifier 10.1109/ACCESS.2016.2553719

Disturbance Rejection by Acceleration Feedforward for Marine Surface Vessels

ØIVIND KÅRE KJERSTAD[1,2,3] AND ROGER SKJETNE[1]

[1]Department of Marine Technology, Norwegian University of Science and Technology, Trondheim 7491, Norway
[2]Department of Civil and Transport Engineering, Norwegian University of Science and Technology, Trondheim 7491, Norway
[3]Arctic Technology Department, The University Centre in Svalbard, Longyearbyen 9171, Norway

Corresponding author: Ø. K. Kjerstad (oivind.k.kjerstad@ntnu.no)

This work was supported in part by the Norges Forskningsråd through the CRI SAMCoT Project under Grant 203471 and through the COE AMOS Project under Grant 223254. in part by the Research Council of Norway through the KMB Project: Arctic DP, with partners Kongsberg Maritime, Statoil, and DNV GL, under Grant 199567, and in part by the MARTEC ERA-NET Project: Dynamic positioning in ice covered waters under Project 196897 which supplied experimental data from the Hamburg Ship Model Basin, and PhD Ivan Metrikin for providing the numerical model and great support.

ABSTRACT Acceleration signals have a powerful disturbance rejection potential in rigid body motion control, as they carry a measure proportional to the resulting force. Yet, they are seldom used, since measuring, decoupling, and utilizing the dynamic acceleration in the control design is not trivial. This paper discusses these topics and presents a solution for marine vessels building on conventional methods together with a novel control law design, where the dynamic acceleration signals are used to form a dynamic referenceless disturbance feedforward compensation. This replaces conventional integral action and enables unmeasured external loads and unmodel dynamics to be counteracted with low time lag. A case study shows the feasibility of the proposed design using experimental data and closed-loop high fidelity simulations of dynamic positioning in a harsh cold climate environment with sea-ice.

INDEX TERMS Marine technology, Closed loop systems, Ice.

I. INTRODUCTION

In marine motion control the main objective is typically to control the position and velocity of a ship to a desired state. This is usually achieved with the structure seen in Figure 1 through model-based control design relying on state measurements of position, heading, and sometimes angular velocity. Such systems have a good track record and are proven stable and robust in a wide range of sea states; see [1] and [2]. Yet, their ability to handle unmodeled dynamics and environmental disturbances is limited to integral action based on state feedback. However, since the state measurements hold time integrals of the force, there is an inherent lag before it propagates significantly to adapt the system. This works well for slowly varying forces, but when rapid and substantial force transients occur the control precision can be severely affected [3]–[5]. How to handle harsh and rapidly varying exogenous disturbances due to loads from sea-ice on a dynamically positioned vessel was the objective of the Arctic DP project [6] that initiated this study.

In general, there are two approaches to dealing with this challenge. The first is extending the model used in control design to describe the additional physics. Yet, modelling

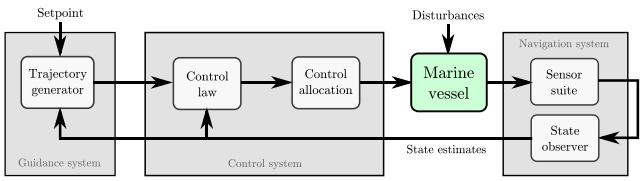

FIGURE 1. Signal flow in guidance, navigation, and control of marine craft. Adapted from [1].

phenomena such as harsh weather, wave trains, equipment in the sea connected to the vessel, current surges, interaction effects with other vessels, and sea-ice interaction may be challenging for control purposes as they are results of complex physical processes. The second approach, which is the topic of this paper, is extending the sensor suite of the vessel to capture the phenomena in question. Here acceleration signals are investigated. These are especially attractive as they carry a proportional measure of the resulting force. Special emphasis is put on dynamic positioning (DP), defined by [7] as automatically maintaining position (fixed location or predetermined track) exclusively through the use of the ship's thrusters alone. It is used in low velocity operations when

a precise geo-fixed or relative position is needed. Examples include cargo transfer between ships and platforms, subsea construction, diving support, drilling, pipelaying, etc.

To apply acceleration signals in the control design require a sensor suite containing accelerometers. The technology itself is well established; see [8] and found in a variety of applications such as consumer electronics, vibration sensing of large structures, impact detection, and navigation. In some cases inertial measurement units (IMUs), containing accelerometers, gyroscopes, and magnetometers are part of marine vessel sensor suites to supply onboard systems with roll and pitch measurements (these are calculated based on the strong influence of gravity on the measurements; see [1]). However, accelerometer measurements are not commonly used in closed-loop motion control. There are several reasons for this, but foremost that the sensor output is not a direct measure of the dynamic acceleration (i.e., the acceleration resulting in motion). The output is dependent on the location of the sensor in the vessel hull and affected by gravity, measurement bias, and sensor noise. An exception is found in [9] where linear motion acceleration signals are used to enhance the state observer for DP and introduce an additional acceleration feedback term in the control law. In our paper the distinction is that the full acceleration vector is found. This enables use of kinematic and sensor models in the state observer, and for forming an acceleration feedforward (AFF) signal used in the control law to directly compensate a disturbance, as previously proposed by the authors in [10] and [11]. This provides a powerful and reactive tool for developing robust control systems operating in harsh environments, where traditional control designs are not well suited.

The main contributions of this paper are the design methodology incorporating AFF in the control law to compensate disturbances and unmodeled dynamics, and experimental verification of the load estimation and the measurement setup showing feasibility of these methods. As the proposed control law design method is novel, a motivating example is given below to showcase its main concept.

Mathematical Notation: In UGS, UGAS, UGES, etc., stands G for Global, S for Stable, U for Uniform, A for Asymptotic, and E for Exponential. Total time derivatives of $x(t)$ are denoted $\dot{x}, \ddot{x}, x^{(3)}, \ldots, x^{(n)}$. The Euclidean vector norm is $|x|$, the induced matrix 2-norm is denoted $\|A\|$, while the signal norm is denoted $\|u\| := sup\{|u(t)| : t \geq 0\}$. Stacking several vectors into one is denoted $\text{col}(x, y, \ldots) \triangleq \left[x^\top, y^\top, \ldots\right]^\top$. The smallest and largest eigenvalues of $A > 0$ is denoted $\lambda_{\min}(A) > 0$ and $\lambda_{\max}(A) > 0$, respectively.

A. MOTIVATING EXAMPLE

To illustrate how AFF is applied in control design, consider a scalar mechanical system with unity mass and nonlinear damping,

$$\ddot{x} + \dot{x}^3 = u + d(t), \tag{1}$$

where $(x, \dot{x}, \ddot{x})$ is the position, velocity, and acceleration – all measured quantities, u is a control input force, and $d(t)$ is an external disturbance force. The objective is to control $x(t)$ to accurately track a desired position $x_d(t)$, where $(x_d(t), \dot{x}_d(t), \ddot{x}_d(t))$ are all bounded and available signals. We assume the disturbance is bounded, absolutely continuous, and $\exists d_m > 0$ such that $\left|\dot{d}(t)\right| \leq d_m$ a.a. $t \geq 0$.

Let the control law be divided into a nominal term Γ and a term Δ to compensate the disturbance, that is,

$$u = \Gamma - \Delta, \tag{2}$$

where the objective of Γ is to ensure nominal closed-loop performance that satisfies the specification of the control problem when $d(t) = 0$, and the objective of Δ is to handle the disturbance $d(t)$.

To design Γ we define a Hurwitz matrix

$$A = \begin{bmatrix} 0 & 1 \\ -k_1 & -k_2 \end{bmatrix}, \tag{3}$$

and let $P = P^\top > 0$ satisfy the Lyapunov equation $PA = A^\top P = -qI$ with $q > 0$. Using $k = [k_1, k_2]$ we assign the nominal term

$$\Gamma(\ddot{x}_d, \dot{x}, e, t) := -ke + \dot{x}^3 + \ddot{x}_d(t), \tag{4}$$

where $e := \text{col}(x - x_d(t), \dot{x} - \dot{x}_d(t))$. Differentiating $V_0(e) = e^\top Pe$ along the solutions of the closed-loop system

$$\dot{e} = Ae + b\left(d(t) - \Delta\right), \tag{5}$$

where $b = \text{col}(0, 1)$, gives

$$\dot{V}_0 = -qe^\top e + 2e^\top Pb\left(d(t) - \Delta\right), \tag{6}$$

and it follows for $d(t) - \Delta = 0$ that $\{e = 0\}$ is UGES. To design Δ we propose two options, direct and filtered acceleration feedforward.

1) DIRECT ACCELERATION FEEDFORWARD

Assume $a(t) = \ddot{x}(t - \delta)$ is the acceleration measurement for (1), where δ is a small known time delay due to signal processing and communication. Then, by direct feedforward, we assign the signal

$$\Delta(t) := a(t) + \dot{x}(t - \delta)^3 - u(t - \delta), \tag{7}$$

which from (1) implies that $\Delta(t) = d(t - \delta)$. Using $p_M = \lambda_{\max}(P)$ it now follows that

$$\begin{aligned} \dot{V}_0 &\leq -q\,|e|^2 + 2p_M\,|e|\,|d(t) - d(t - \delta)| \\ &\leq -\frac{q}{2}\,|e|^2 + \Lambda\delta^2, \end{aligned} \tag{8}$$

where $\Lambda := 2\frac{p_M^2 d_m^2}{q}$, and using the Global Lipschitz property $|d(t) - d(\tau)| \leq d_m\,|t - \tau|$ (following from absolute continuity of $d(t)$ and boundedness of $\dot{d}(t)$). Letting $\tilde{d}(t) := d(t) - d(t - \delta)$, (8) implies that the resulting closed-loop system

$$\dot{e} = Ae + b\tilde{d}(t) \tag{9}$$

is input-to-state stable (ISS) with respect to $\tilde{d}(t)$ and, correspondingly, the delay δ. A small delay $\delta \ll 1$ will from (8)

result in a small impact by the disturbance on the tracking performance. In the limit as $\delta \to 0$ the difference $\tilde{d}(t)$ vanishes and the nominal performance is recovered.

Note that an alternative to (4) and (7) is to use the simpler control law

$$\Gamma(\ddot{x}_d, e, t) := -ke + \ddot{x}_d(t) \tag{10a}$$
$$\Delta(t) := a(t) - u(t-\delta) \tag{10b}$$
$$= d(t-\delta) - \dot{x}(t-\delta)^3, \tag{10c}$$

which shows that the feedforward term Δ can be realized model-free, without knowledge of the velocity. Instead, the nonlinear damping term is accounted for in the extended disturbance $\bar{d}(t) = d(t) - \dot{x}(t)^3$ such that $\tilde{d}(t) = \bar{d}(t) - \bar{d}(t-\delta)$, and the same conclusion follows. This is important as it allows for handling uncertain or unmodeled dynamics.

2) FILTERED ACCELERATION FEEDFORWARD

Now let Δ be the state of a filter to track $d(t)$ as closely as possible. In this case, the control law (2) becomes dynamic, where Γ is defined in (4). Letting $\varepsilon := d(t) - \Delta$ be the disturbance tracking error, and differentiating

$$V(e, \varepsilon) = V_0(e) + \frac{1}{2}\varepsilon^2 \tag{11}$$

along the solutions of (5) and $\dot{\Delta}$ gives

$$\dot{V} = -qe^\top e + \left(2e^\top Pb + \dot{d}(t) - \dot{\Delta}\right)\varepsilon. \tag{12}$$

Assuming now there is no time delay on the state measurements, and using $a(t) = \ddot{x}(t)$, we notice from (1) and (2) that $\varepsilon = \ddot{x} + \dot{x}^3 - \Gamma$. We assign

$$\dot{\Delta} = 2b^\top Pe - \mu\left(\Gamma - a - \dot{x}^3\right)$$
$$= 2b^\top Pe - \mu\varepsilon. \tag{13}$$

The derivative of (11) along the solutions of the resulting closed-loop system

$$\dot{e} = Ae + b\varepsilon \tag{14}$$
$$\dot{\varepsilon} = -2b^\top Pe - \mu\varepsilon + \dot{d} \tag{15}$$

now becomes

$$\dot{V} = -qe^\top e - \mu\varepsilon^2 + \varepsilon\dot{d}(t)$$
$$\leq -q\,|e|^2 - \frac{\mu}{2}\,|\varepsilon|^2 + \frac{1}{2\mu}\,|\dot{d}(t)|^2, \tag{16}$$

which shows that the system is ISS with respect to $\dot{d}(t)$ as a disturbance input, where the filter gain μ can be used to attenuate its impact on the closed-loop tracking performance.

Note again that we can remove the nonlinear damping term $\dot{x}^3$ from (4) and (13), incorporate it into the extended disturbance $\bar{d}(t) = d(t) - \dot{x}(t)^3$, and arrive at a model-free control law with Γ from (10a) and

$$\dot{\Delta} = 2b^\top Pe - \mu\,(\Gamma - a) \tag{17a}$$
$$u = \Gamma - \Delta. \tag{17b}$$

Inserting (10a) into (17a) we notice that Δ serves as an integral action state on the augmented error $\bar{e} = \mathrm{col}(e, \dot{x} - \dot{x}_d(t))$.

3) SIMULATION COMPARISON

To further showcase AFF control design, a simulation of (1) with $d(t)$ of increasing severity is presented. Three control laws, each with two parameter variations, were used for a point stabilization objective ($x_d = 0$). The compared control laws were:

- The nominal control law (4) together with direct AFF (7), using high and low δ.
- The nominal control law (4) together with filtered AFF (13), using high and low μ.
- A PID control law, $u = -ke - k_i \int e dt$, where $k_i = [k_{i1}, k_{i2}]$, with high and low k_i.

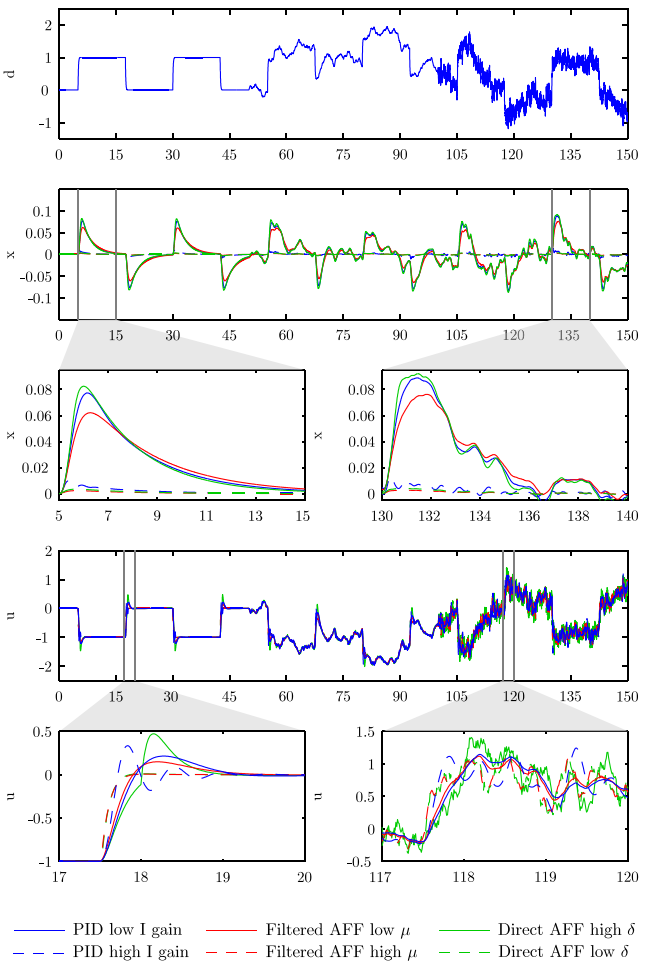

FIGURE 2. Top: the time development of the state subject to different control strategies. Notice that the disturbance signal is marked by light blue. Bottom: a close-up of the control input.

All of the above were simulated using fixed common nominal control gains $k = [2, 5]$. Figure 2 shows $d(t)$ in the top plot, and the tracking performance of x and control input u in the subsequent. The AFF control laws with low disturbance attenuation (high δ or low μ) offers no real advantage over PID as the performance is comparable. However, increasing the integral action of the PID to improve the disturbance rejection eventually results in control input oscillations.

This is best seen in the lower left plot. The AFF control laws with high disturbance attenuation (low δ and high μ) does not have this problem. They are able to accurately attenuate the disturbance, recovering the nominal performance, without control input oscillations. Improved control precision is thus obtained.

II. PROBLEM FORMULATION

For 3 degrees-of-freedom (DOF) motion control of a rigid-body marine surface vessel, we consider a generalization of the state-of-the-art models [1], [2],

$$\dot{\eta} = R(\psi)\nu \tag{18a}$$

$$M\dot{\nu} = \tau + \rho(\eta, \nu) + d(t) \tag{18b}$$

where $\eta = \text{col}\,(x, y, \psi) \in \mathbb{R}^3$ is the position and orientation of the body in the inertial frame, $\nu = \text{col}\,(u, v, r) \in \mathbb{R}^3$ is the body-fixed linear and angular velocity of the body, $M = M^\top > 0$ is the rigid body inertia matrix, $\tau \in \mathbb{R}^3$ is the body-fixed control input, $\rho : \mathbb{R}^3 \times \mathbb{R}^3 \to \mathbb{R}^3$ is a locally Lipschitz function containing nonlinear dynamics (Coriolis, damping, and restoring forces), and $d : \mathbb{R}_{\geq 0} \to \mathbb{R}^3$ accounts for external time-varying disturbances. We assume $\exists d_m > 0$ such that $\max\{\|d(t)\|, \|\dot{d}(t)\|\} \leq d_m$. $R(\psi) \in SO(3)$ is the rotation matrix between the body frame and the inertial frame. This has the following properties,

$$R(\psi)^\top R(\psi) = R(\psi)R(\psi)^\top = I \tag{19}$$

$$\dot{R} = R(\psi)S(r) \tag{20}$$

where $S(r) \in \mathbb{R}^{3\times 3}$ is a skew symmetric matrix with the following properties,

$$S(r) = \begin{bmatrix} 0 & -r & 0 \\ r & 0 & 0 \\ 0 & 0 & 0 \end{bmatrix} = -S(r)^\top. \tag{21}$$

For control design we assume that the following signals are available: The vessel position, $p = \text{col}\,(x, y, z) \in \mathbb{R}^3$, measured in the assumed inertial north-east-down (NED) frame. The vessel orientation, $\Theta = \text{col}\,(\phi, \theta, \psi) \in \mathbb{R}^3$, measured in the body frame relative to the NED frame. The vessel rate of turn, $\omega = \text{col}\,(p, q, r) \in \mathbb{R}^3$, measured in the body frame relative to the NED frame. And finally, accelerometer output $a_m = \text{col}\left(a_x, a_y, a_z\right)$ measured on the rigid body in its sensor frame relative to the NED frame.

In this paper we refer to an accelerometer as a body-fixed three axis orthogonal linear sensor. By assuming that the accelerometer is aligned with the body frame, and that the sensor scale-factor, cross-coupling, and misalignment errors are negligible after calibration, we modeled it as in [12],

$$a_m = a_l + \omega \times v + g + b + w \tag{22a}$$

$$\dot{g} = -\omega \times g \tag{22b}$$

where $a_m \in \mathbb{R}^3$ is the sensor output, $a_l \in \mathbb{R}^3$ is the linear dynamic acceleration in the sensor mounting point, $\omega = \text{col}\,(p, q, r)$ is the angular rate of the body relative to the inertial frame, and $v = \text{col}\,(u, v, w)$ is linear velocity of the body. Notice that v in (18) contains elements of both v and ω. Furthermore, $g \in \mathbb{R}^3$ is the gravitational component expressed in the body frame, $b \in \mathbb{R}^3$ is the sensor bias, and $w \in \mathbb{R}^3$ is the sensor noise.

To enable use of the dynamic acceleration in control design, three challenges must be overcome. The first is that it may be impractical, or even impossible, to mount a sensor in the point of control. Here the point of control will be referred to as origin (CO) of the body frame. What arises is a dependency on the distance between CO and the sensor mounting position given by

$$a_l = a_{\text{co}} + \alpha \times l + \omega \times (\omega \times l) \tag{23}$$

where $a_{\text{co}} \in \mathbb{R}^3$ is the linear dynamic acceleration in CO, $\alpha \in \mathbb{R}^3$ is the angular acceleration, and $l \in \mathbb{R}^3$ is the body frame distance vector between the points of measure and CO. The latter will be referred to as the accelerometer lever arm, or just lever arm.

The second challenge is the fact that $a_{\text{co}} \neq \dot{\nu}$. The dynamic acceleration a_l captured in an accelerometer (along with other effects) does not contain the angular acceleration α. It should be mentioned that sensors capable of measuring α exists [8], but they are not common in marine applications. Therefore, such are not considered here. We propose to obtain α through exploiting the lever arm dependency of four distributed accelerometers. Thus, the third challenge is that of acquiring $\dot{\nu}$ from these.

The main objective is to design a 3 DOF control law τ for (18) utilizing $\dot{\nu}$, using the state-of-the-art structure of Figure 1, such that the vessel accurately tracks a predefined time-parametrized trajectory given by $\{\eta_d(t), \nu_d(t), \dot{\nu}_d(t)\}$ while subject to unmodeled dynamics and rapidly varying disturbances. Although the control design will provide the main contribution, the application of acceleration measurements must be given attention to tackle the aforementioned challenges in both the sensor suite and the state estimation.

Since solving the three challenges to obtain the dynamic acceleration is a prerequisite for the control design, the paper is structured likewise. Chapter 3 presents the reconstruction of the dynamic acceleration through multiple accelerometers and a state observer. Chapter 4 derives and analyzes dynamic tracking control laws based on filtered AFF. Chapter 5 features a case study investigating DP subject to severe ice interaction in an Arctic operation. Finally, Chapter 6 summarizes and concludes the results of the paper.

III. RECONSTRUCTING THE DYNAMIC ACCELERATION

To overcome the two first challenges of using accelerometers we exploit four spatially distributed sensors and the relation between them. This enables use of well known, matured, and relatively cheap and rugged conventional accelerometers in a spatial configuration to setup a virtual 6 DOF accelerometer in CO. Similar schemes are seen in [13] and [14]. The final accelerometer challenge of obtaining $\dot{\nu}$ is handled by reformulating the state observer. Although the control objective of this paper does not require the 6 DOF acceleration vector,

it is practical for the removal of gravity and for generality to include it.

A. 6 DOF ACCELERATION MEASUREMENT

Consider parameterizing (23) as a product of its static and dynamic variables

$$a_l = \begin{bmatrix} I_{3\times 3} & S(l)^\top & H(l) \end{bmatrix} \begin{bmatrix} a_{\text{co}} \\ \alpha \\ \bar{\omega} \end{bmatrix} \tag{24a}$$

$$= W(l)z. \tag{24b}$$

where $I_{3\times 3} \in \mathbb{R}^{3\times 3}$ is an identity matrix, $S(l)$ is given in (21), and

$$H(l) = \begin{bmatrix} 0 & -l_x & -l_x & l_y & l_z & 0 \\ -l_y & 0 & -l_y & l_x & 0 & l_z \\ -l_z & -l_z & 0 & 0 & l_x & l_y \end{bmatrix}, \tag{25}$$

is a sub-matrix of the accelerometer configuration matrix $W(l) \in \mathbb{R}^{3\times 12}$, and $z \in \mathbb{R}^{12}$ is the linear acceleration, angular acceleration, and angular rate cross product vector. The latter contains $\bar{\omega} \in \mathbb{R}^6$ defined as

$$\bar{\omega} = \begin{bmatrix} \omega_x^2 & \omega_y^2 & \omega_z^2 & \omega_x\omega_y & \omega_x\omega_z & \omega_y\omega_z \end{bmatrix}^\top. \tag{26}$$

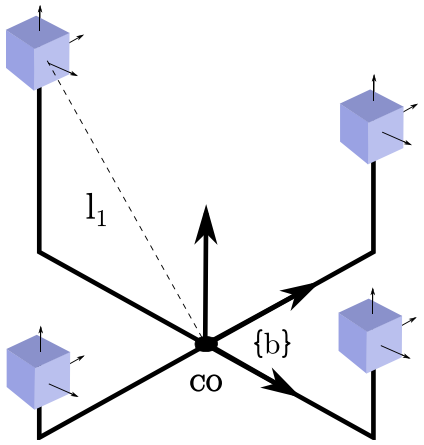

FIGURE 3. An illustration of one possible setup of the accelerometers for measuring the full state acceleration vector.

As mentioned, by measuring in one location $W(l)$ cannot be inverted to find z. Therefore, we propose to use a configuration of four sensors, as illustrated in Figure 3, such that (24b) can be extended to

$$\begin{bmatrix} a_{l1} \\ a_{l2} \\ a_{l3} \\ a_{l4} \end{bmatrix} = \begin{bmatrix} W(l_1) \\ W(l_2) \\ W(l_3) \\ W(l_4) \end{bmatrix} z \tag{27}$$

$$a_c = G(l_c)z \tag{28}$$

where $a_c \in \mathbb{R}^{12}$ is the combined linear acceleration vectors in the sensor mounting positions, $G(l_c) \in \mathbb{R}^{12\times 12}$ is the combined sensor configuration matrix and $l_c = col(l_1, l_2, l_3, l_4)$ is the combined sensor lever arm vector. To calculate z it is important to ensure that the static matrix $G(l_c)$ is nonsingular. According to [15], this is achieved when the sensors are oriented equally and their positions are not co-planar, that is at least one sensor must not lie in the same plane as the three others. Then, by substituting in the four accelerometer equations in (22a) for a_c, we get

$$G^{-1}a_{mc} = z + G^{-1} \begin{bmatrix} \omega \times v + g + b_1 + w_1 \\ \omega \times v + g + b_2 + w_2 \\ \omega \times v + g + b_3 + w_3 \\ \omega \times v + g + b_4 + w_4 \end{bmatrix}, \tag{29}$$

where $a_{mc} = col(a_{m1}, a_{m2}, a_{m3}, a_{m4})$. This shows that the setup with four spatially distributed accelerometers constitutes a virtual 6 DOF sensor placed in CO. Notice that it still has the same sensor effects as (22a) on the measurements.

FIGURE 4. R/V Gunnerus and a MRU 5+. Courtesy of Fredrik Skoglund, and Kongsberg Seatex.

TABLE 1. Placement of MRUs in R/V Gunnerus relative to CO.

Nr.	X [m]	Y [m]	Z [m]	Note
1	0.358	0.804	-4.321	Technical room
2	14.978	0.039	0.568	Bow bulb
3	-7.454	4.123	-0.012	Engine room stb.
4	-7.545	-4.251	-0.730	Engine room port

B. EXPERIMENTAL VERIFICATION

In November 2013 a series of maneuvering experiments were carried out with the NTNU research vessel Gunnerus offshore mid-Norway. Four Kongsberg Seatex 5+ Motion-Refecence Units (MRUs) [16] were installed onboard. The vessel and sensor are seen in Figure 4. Prior to the campaign, the MRU's lever arms and orientation were accurately measured using laser-based industrial surveying techniques [17]. Table 1 shows the MRU positions.

The MRUs were placed in the vessel hull such that $G(l_c)$ was nonsingular and spatially large. By investigation of the eigenvalues of $G(l_c)^{-1}$ it was found that they were of magnitude less than one. From (29) this implies improved noise and bias attenuation. Both a_l and ω were logged from each MRU at 100 Hz by a Kongsberg Seatex Vessel Motion Monitor (VMM). Notice that a_l, and not a_m was logged. This was due to a proprietary undisclosed algorithm providing the necessary compensation internally in the MRUs.

Figure 5 features the output of the 6 DOF measurement setup compared to MRU 1 data from when Gunnerus performed a turning circle in multi-directional swell waves with

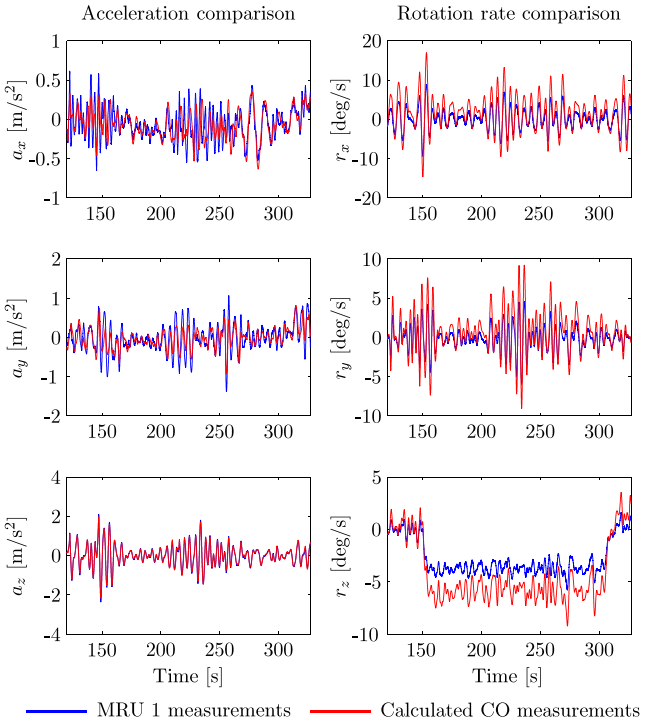

FIGURE 5. Comparison of the obtained acceleration vector with data output of MRU 1. Left column: The multi-sensor linear accelerations vs. MRU 1 output. Right column: The multi-sensor integration of the angular accelerations vs. MRU 1 gyroscope output.

significant wave height of 2.1 m and period of 8.5 s. The left column shows the calculated a_{co} compared to MRU 1 a, and the right, $\int \alpha\, dt$ compared to MRU 1 ω.

The results show that the oscillatory wave induced components of the calculated output match well. The deviations in magnitude are believed to stem from the MRU 1 elevated position coupled with roll and pitch motions. In the right column, the angular acceleration is compared to the MRU 1 gyroscope by integration. Although seemingly biased and deviating in magnitude, the oscillatory components of the signals match well, indicating the feasibility of measuring the angular acceleration component.

C. STATE OBSERVER

In order to solve the last accelerometer challenge, and obtain $\dot{\nu}$, the state observer of Figure 1 is redefined from an implementation of (18) [2] to a model including and exploiting the acceleration measurement system. The structure applied is shown in Figure 6, and the model is

$$\dot{p}_v = -S(\omega(t))p_v + v \tag{30a}$$
$$\dot{v} = -S(\omega(t))v - b_l - g + B_1 G^{-1} a_{mc} \tag{30b}$$
$$\dot{g} = -S(\omega(t))g \tag{30c}$$
$$\dot{b}_l = 0 \tag{30d}$$
$$\dot{\omega} = b_\omega + B_2 G^{-1} a_{mc} \tag{30e}$$
$$\dot{b}_\omega = 0, \tag{30f}$$

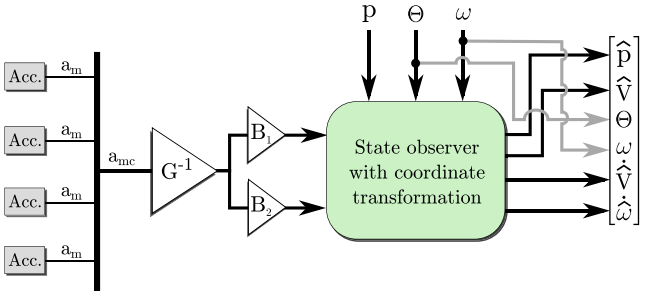

FIGURE 6. Block diagram showing the relation between the accelerometer sensor suite and the state observer.

where $p_v := R(\Theta)^\top p$ is the position rotated to the body frame, $v = col(u, v, w) \in \mathbb{R}^3$ is the linear velocity subsystem, $a_{mc} \in \mathbb{R}^{12}$ is the collective accelerometer measurement vector, as seen in (29), $b_l \in \mathbb{R}^3$ and $b_\omega \in \mathbb{R}^3$ are the linear and rotational accelerometer bias originating from the sensor transformation, and $B_{1,2} \in \mathbb{R}^{3\times 12}$ are selection matrices for a_{co} and α, respectively.

This redefinition has two important aspects. The first is that it allows for full state feedback control design including $\dot{\nu}$. Thus, AFF designs similar to those presented in the motivational example can be applied. The second is that it improves the tracking capability of the observer. If unmodeled dynamics and harsh disturbances are not handled, poor state estimation will occur, which in turn results in reduced control accuracy. By replacing the kinetic model (18b) with a model composed of kinematic and sensor characteristics (30b)-(30f) the acceleration signal, capturing the system dynamics through measurements, acts as input to the state observer. The performance is therefore not dependent on model assumptions and validity for the given environment, but rather on the quality of the sensor suite. For DP this is especially attractive as reduced state estimation performance has been reported [3], [18], and [5].

As the above model contains cross products between the states ω and p_v, v, and g, respectively, it is nonlinear. State-of-the-art observer designs for nonlinear systems includes various nonlinear extensions of the Kalman filter. The downside with these is the lack of established convergence and stability properties. Here a work around is applied. In (30) the objective of the ω state is to remove bias from α. It is assumed that ω is available with high precision and low noise characteristics. This is reasonable as most marine crafts carry a high end attitude systems capable of supplying both Θ and ω. Therefore, by regarding it as a time-varying signal in the position and linear velocity subsystems (30a)-(30c) the nonlinear model can be regarded as linearly time varying (LTV), and written as

$$\dot{x} = A(t)x + BG^{-1}a_m \tag{31}$$
$$y = \begin{bmatrix} p_v & \omega \end{bmatrix}^\top, \tag{32}$$

where $x = \text{col}(p_v, v, b_l, g, \omega, b_\omega)$. For LTV systems a wide range of Kalman-related results are available;

see [19], [20], and [21]. The solution in [22], with the state vector extended by ω and b_ω, is chosen to solve the estimation problem.

An aspect of (30b) is that it holds two competing integrators in b_l and g. In [12], the subsystem (30a)-(30d) is found uniformly completely observable iff $\omega(t)$ has sufficient perturbations (with $y = p_v$). Although this cannot be guaranteed at all times, it does not constitute a problem as the collective bias $b_l + g$ is uniformly completely observable. Thus, the estimation performance of determining p_v, v, a_{co}, and α is not compromised.

In summary, all the three accelerometer challenges have been investigated and solved, catering for realization of AFF control law designs utilizing full state feedback including $\dot{v}$.

IV. CONTROL DESIGN

The role of the control law in Figure 1 is to calculate the 3 DOF control efforts needed to fulfill the control objective of making η track a desired vector $\eta_d((t)$ in NED. Thus, the control designs presented in this section employ only the planar subset of signals supplied by the sensor suite and state observer (i.e., η, ν, and $\dot{\nu}$).

Since marine vessels propulsion typically are unsymmetrical with respect to the yz-plane, it is convenient to tune the positioning response of the control law with respect to vessel-parallel (VP) coordinates. Correspondingly, we transform the position/heading vector η from NED to VP, that is, $\eta_v := R(\psi)^\top \eta$.

We define $\eta_{v,d} := R(\psi)^\top \eta_d(t)$, resulting in the VP error state

$$\begin{aligned}\tilde{\eta}_v &= \eta_v - \eta_{v,d} \\ &= R(\psi)^\top (\eta - \eta_d(t)) \\ &= R(\psi)^\top \tilde{\eta}, \end{aligned} \tag{33}$$

where $\tilde{\eta} := \eta - \eta_d(t)$. We similarly define

$$v_d := R(\psi)^\top \dot{\eta}_d(t) \tag{34a}$$

$$a_d := \dot{v}_d = -S(r)v_d + R(\psi)^\top \ddot{\eta}_d(t), \tag{34b}$$

and $\tilde{\nu} := \nu - \nu_d(t)$, where we used $\dot{R} = R(\psi)S(r)$ and $S(r) = -S(r)^\top$. This yields the error dynamics

$$\dot{\tilde{\eta}}_v = -S(r)\tilde{\eta}_v + \tilde{\nu} \tag{35a}$$

$$M\dot{\tilde{\nu}} = \tau + \rho(\eta, \nu) + d(t) - Ma_d. \tag{35b}$$

To achieve disturbance rejection by AFF, we propose the following control law

$$\tau = \Gamma - \Delta \tag{36}$$

where $\Gamma : \mathbb{R}_{\geq 0} \times \mathbb{R}^n \times \mathbb{R}^n \to \mathbb{R}^n$ is a nominal control law, and $\Delta \in \mathbb{R}^n$ is a dynamic disturbance attenuation state. Correspondingly, $\varepsilon := d(t) - \Delta$ defines a disturbance rejection error signal.

A. NOMINAL TRACKING DESIGN

We consider first the nominal design, where ε is considered a disturbance input from which we want to render the system input-to-state stable (ISS). The design of the term Δ is left for later. The objective is thus to design a nominal control law for Γ that renders the closed-loop system UGES for the case $\varepsilon = 0$ and ISS for $\varepsilon \neq 0$.

A common approach to achieve UGES is to apply a backstepping-based transformation of the state. Accordingly, we define the linear state transformation $z := \mathrm{col}(z_1, z_2)$ with $z_1 := \tilde{\eta}_v$ and $z_2 := \tilde{\nu} + K_1\tilde{\eta}_v$. Defining $\tilde{x} := \mathrm{col}(\tilde{\eta}_v, \tilde{\nu})$, and letting $K_1 = K_1^\top > 0$ and $K_2 = K_2^\top > 0$ be feedback gain matrices, we get the following proposition based on conventional backstepping.

Proposition 1: There exist positive constants k, λ, and γ such that the solutions of the closed-loop system (35) with the control (36) and

$$\begin{aligned}\Gamma = &-[I + K_2K_1 - MK_1S(r)]\,\tilde{\eta}_v \\ &-[K_2 + MK_1]\,\tilde{\nu} - \rho(\eta, \nu) + Ma_d, \end{aligned} \tag{37}$$

satisfies the uniform bound

$$|\tilde{x}(t)| \leq \max\left\{k\,|\tilde{x}(t_0)|\,e^{-\lambda(t-t_0)},\ \gamma \sup_{t_0\leq\tau\leq t}\|\varepsilon(\tau)\|\right\}. \tag{38}$$

Proof: The control law (37) can be rewritten in the z-states as

$$\begin{aligned}\Gamma = &-z_1 - K_2z_2 - \rho(\eta, \nu) + Ma_d \\ &-MK_1\,(\tilde{\nu} - S(r)\tilde{\eta}_v)\,, \end{aligned} \tag{39}$$

such that the closed-loop system becomes

$$\dot{z}_1 = -S(r)z_1 - K_1z_1 + z_2 \tag{40a}$$

$$M\dot{z}_2 = -z_1 - K_2z_2 + \varepsilon. \tag{40b}$$

Differentiating the Lyapunov function

$$V(z) = \frac{1}{2}z_1^\top z_1 + \frac{1}{2}z_2^\top Mz_2 \tag{41}$$

along the solutions of (40), we get

$$\begin{aligned}\dot{V} &= -z_1^\top K_1z_1 - z_2^\top K_2z_2 + z_2^\top\varepsilon \\ &\leq -2c_3\,|z|^2 + |z|\,|\varepsilon| \\ &\leq -c_3\,|z|^2\,, \quad \forall\,|z| \geq \frac{1}{c_3}\,|\varepsilon| \end{aligned} \tag{42}$$

where $c_3 = \frac{1}{2}\lambda_{\min}(K_1, K_2)$. We also have $c_1\,|z|^2 \leq V(z) \leq c_2\,|z|^2$ where $c_1 = \frac{1}{2}\min\{1, \lambda_{\min}(M)\}$ and $c_2 = \frac{1}{2}\max\{1, \lambda_{\max}(M)\}$. It follows from ISS theorems [23, Theorem 4.6] that the solutions in the z-coordinates satisfy

$$|z(t)| \leq max\left\{\sqrt{\frac{c_2}{c_1}}\,|z(t_0)|\,e^{-\frac{c_3}{c_2}(t-t_0)},\ \frac{c_2}{c_1c_3}\sup_{t_0\leq\tau\leq t}\|\varepsilon(\tau)\|\right\}. \tag{43}$$

The state transformation can be written $z = T\tilde{x}$ where

$$T := \begin{bmatrix} I & 0 \\ K_1 & I \end{bmatrix}, \quad T^{-1} = \begin{bmatrix} I & 0 \\ -K_1 & I \end{bmatrix}, \tag{44}$$

and

$$T^\top T = \begin{bmatrix} I + K_1^\top K_1 & K_1^\top \\ K_1 & I \end{bmatrix} > 0. \tag{45}$$

Letting $\sigma_1 := \sqrt{\lambda_{\min}\left(T^\top T\right)}$ and $\sigma_2 := \sqrt{\lambda_{\max}\left(T^\top T\right)}$ gives[1] the equivalence relation

$$\sigma_1 |\tilde{x}| \le |z| \le \sigma_2 |\tilde{x}|. \tag{46}$$

For the exponential convergence bound in (43) we get

$$|\tilde{x}(t)| \le \frac{\sigma_2}{\sigma_1}\sqrt{\frac{c_2}{c_1}}\,|\tilde{x}(t_0)|\, e^{-\frac{c_3}{c_2}(t-t_0)}, \tag{47}$$

and for the input bound we get

$$|\tilde{x}(t)| \le \frac{c_2}{\sigma_1 c_1 c_3} \sup_{t_0 \le \tau \le t} \|\varepsilon(\tau)\|. \tag{48}$$

Hence, we take $k = \frac{\sigma_2}{\sigma_1}\sqrt{\frac{c_2}{c_1}}$, $\lambda = \frac{c_3}{c_2}$, and $\gamma = \frac{c_2}{\sigma_1 c_1 c_3}$. □

A slightly different control law can be derived from LgV-backstepping [24].

Proposition 2: There exist positive constants k, λ, and γ such that the solutions of the closed-loop system (35) with the control (36) and

$$\begin{aligned}\Gamma = &-[K_2K_1 - MK_1S(r)]\,\tilde{\eta}_v - [K_2 + MK_1]\,\tilde{\nu} \\ &- \rho(\eta, \nu) + Ma_d,\end{aligned} \tag{49}$$

satisfies the uniform bound (38), where $K_1 = C_1 + \kappa_1 I$ and $K_2 := C_2 + \frac{1}{4\kappa_1} I$ with $C_1 = C_1^\top > 0$, $C_2 = C_2^\top > 0$, and $\kappa_1 > 0$.

Proof: We use $z = \mathrm{col}(z_1, z_2)$, $z = T\tilde{x}$ where T is defined by (44), such that the control law (49) becomes

$$\Gamma = -K_2 z_2 - \rho + Ma_d - MK_1\left(\tilde{\nu} - S\tilde{\eta}_v\right), \tag{50}$$

such that the closed-loop system becomes

$$\dot{z}_1 = -S(r)z_1 - K_1 z_1 + z_2 \tag{51a}$$

$$M\dot{z}_2 = -K_2 z_2 + \varepsilon. \tag{51b}$$

Differentiating the Lyapunov function (41) along the solutions of (51), we get

$$\begin{aligned}\dot{V} &\le -z_1^\top C_1 z_1 - z_2^\top C_2 z_2 + z_2^\top \varepsilon \\ &\le -\bar{c}_3 |z|^2, \quad \forall\, |z| \ge \frac{1}{\bar{c}_3}|\varepsilon|\end{aligned} \tag{52}$$

where $\bar{c}_3 = \frac{1}{2}\lambda_{\min}(C_1, C_2)$. The proof hereafter follows the proof of Proposition 1, resulting in the constants $k = \frac{\sigma_2}{\sigma_1}\sqrt{\frac{c_2}{c_1}}$, $\lambda = \frac{\bar{c}_3}{c_2}$, and $\gamma = \frac{c_2}{\sigma_1 c_1 \bar{c}_3}$. □

Contrary to (40), we notice that the closed-loop system (51) makes out a cascade, where the z_2-subsystem for $\varepsilon = 0$ independently converges exponentially to zero while driving the exponentially stable z_1-subsystem. The disturbance rejection error ε will affect this exponential convergence, where ε is first lowpass-filtered through the z_2-dynamics with steady-state gain K_2^{-1} before affecting the tracking error $z_1 = \tilde{\eta}_v$.

[1]Note that σ_1 and σ_2 correspond to the minimum and maximum singular values of $T^\top T$.

B. CLOSING THE LOOP WITH DISTURBANCE REJECTION

While the static part of the control law is given by (36) with either (37) or (49), we will now consider a dynamic filtered design to make the disturbance rejection AFF term Δ track the disturbance $d(t)$ as closely as possible. Towards this end we will apply the 3 DOF dynamic acceleration signal vector $a(t) = \dot{\nu}(t) \in \mathbb{R}^3$ as a feedforward signal for disturbance rejection.

By applying (36) with either of the control laws in propositions 1 or 2, we get the error dynamics

$$\dot{z} = A(r)z + B\varepsilon \tag{53}$$

where $A(r)$ and B are defined from (40) or (51), respectively. Moreover, letting $P := \frac{1}{2}\,\mathrm{diag}\,(I, M)$ and $Q := \mathrm{diag}\,(K_1, K_2)$ for (42) or $Q := \mathrm{diag}\,(C_1, C_2)$ for (52), then in both cases above we have

$$V(z) = z^\top P z \tag{54}$$

$$\dot{V} \le -z^\top Q z + 2z^\top PB\varepsilon, \tag{55}$$

and we have shown that the system is UGES for $\varepsilon = 0$ and ISS with linear gain from ε as input.

1) DIRECT FILTERED DESIGN

With ε defined above as the disturbance rejection error state, we get

$$\dot{\varepsilon} = -\dot{\Delta} + \dot{d}(t). \tag{56}$$

Noting that

$$\varepsilon = d - \Delta = Ma(t) - \Gamma - \rho(\eta, \nu) \tag{57}$$

is an available feedforward signal due to the acceleration measurement, this gives the immediate choice

$$\dot{\Delta} = \mu\left(Ma(t) - \Gamma - \rho(\eta, \nu)\right) \tag{58a}$$

$$= \mu\varepsilon \tag{58b}$$

$$= -\mu\left(\Delta - d(t)\right) \tag{58c}$$

which results in the closed-loop system (53) and

$$\dot{\varepsilon} = -\mu\varepsilon + \dot{d}(t). \tag{59}$$

Theorem 3: The origin $(z, \varepsilon) = (0, 0)$ of the closed-loop system (53) and (59) is UGES for $\dot{d}(t) = 0$ and ISS with $\dot{d}(t)$ as a bounded input.

Proof: UGES of the origin for $\dot{d} = 0$ is concluded since the closed-loop error system (53) and (59) is a cascade of two UGES subsystems connected with linear gain [23, Appendix C]. From converse Lyapunov theorems [23] there then exists a quadratic Lyapunov function, which becomes an ISS-Lyapunov function with $\dot{d}$ as input. □

With the disturbance rejection filter (58), Δ will attempt to track $d(t)$ with accuracy dependent on the gain μ. If $\dot{d}(t) = 0$ then Δ will exponentially converge to and track d as a type of integral action. For $\dot{d}$ nonzero there will be a tracking error, tunable by the gain μ; however, the previous section shows that the nominal DP control laws (37) or (49) render the DP closed-loop system robust to this deviation.

Another choice is to define the CLF

$$W(z,\varepsilon) := V(z) + \frac{1}{2\mu}\varepsilon^\top\varepsilon. \tag{60}$$

Taking the total time derivative along (53) and (59) yields

$$\dot{W} \leq -z^\top Qz + \varepsilon^\top\left(\frac{1}{\mu}\dot{d} - \frac{1}{\mu}\dot{\Delta} + 2B^\top Pz\right).$$

Noting that $PB = \frac{1}{2}\,\mathrm{col}(0, I)$, we assign

$$\dot{\Delta} = \mu\left[Ma(t) - \Gamma - \rho(\eta,\nu) + z_2\right] \tag{61a}$$
$$= \mu\left[\varepsilon + z_2\right] \tag{61b}$$
$$= -\mu\left(\Delta - d(t)\right) + z_2, \tag{61c}$$

which gives

$$\dot{W} \leq -z^\top Qz - \varepsilon^\top\varepsilon + \frac{1}{\mu}\varepsilon^\top\dot{d}. \tag{62}$$

The resulting closed-loop error system becomes (53) and

$$\dot{\varepsilon} = -\mu\varepsilon - \mu z_2 + \dot{d}. \tag{63}$$

Theorem 4: The origin $(z,\varepsilon) = (0,0)$ of the closed-loop system (53) and (63) is UGES for $\dot{d}(t) = 0$ and ISS with $\dot{d}(t)$ as a bounded input.

Proof: The conclusion follows from $W(z,\varepsilon)$ being a quadratic ISS-Lyapunov function with $\dot{d}$ as input. □

2) FILTERED DESIGN BASED ON A DISTURBANCE MODEL

Suppose the disturbance is generated by an exogenous model

$$\dot{\xi} = A_d\xi + E_d w \tag{64a}$$
$$d = C_d\xi \tag{64b}$$

where $\xi \in \mathbb{R}^q$, $q \geq 3$, is the disturbance state, d is the output that affects the DP control system, w is Gaussian white noise, (A_d, E_d, C_d) are linear matrices, and (C_d, A_d) is an observable pair.

Assuming $w = 0$, we design a Luenberger-type disturbance observer

$$\dot{\hat{\xi}} = A_d\hat{\xi} + L_d\varepsilon \tag{65a}$$
$$\Delta = C_d\hat{\xi}, \tag{65b}$$

where the injection signal $\varepsilon = C_d\tilde{\xi} = C_d(\xi - \hat{\xi})$ is generated from (57), and L_d is designed such that $F_d := A_d - L_dC_d$ is Hurwitz. Correspondingly, let $P_d = P_d^\top > 0$ satisfy $P_dF_d + F_d^\top P_d = -Q_d$. This gives the closed-loop system

$$\dot{z} = A(r)z + BC_d\tilde{\xi} \tag{66a}$$
$$\dot{\tilde{\xi}} = F_d\tilde{\xi}. \tag{66b}$$

Theorem 5: The origin $(z,\tilde{\xi}) = (0,0)$ of the closed-loop system (66) is UGES.

Proof: A cascade of two UGES subsystems connected through a linear gain is UGES [23, Appendix C]. □

We note that the disturbance rejection filter (65) can be rewritten as

$$\dot{\hat{\xi}} = F_d\hat{\xi} + L_d d(t) \tag{67a}$$
$$\Delta = C_d\hat{\xi}. \tag{67b}$$

Comparing this to the direct filter design in (58), we recognize $C_d = I$, $L_d = \mu I$, and $A_d = 0$ (such that $F_d = -\mu I$). This indicates that (65) is a general filter that, even if the model (64a) is uncertain or unknown, can be designed to improve the filtering performance of the acceleration feedforward-based injection signal ε from (57). However, the more accurately (64a) models the disturbance, the better tracking of the disturbance is achieved.

C. A NOTE ON THE SEPARATION PRINCIPLE

Since the vessel dynamics (18) is nonlinear and the control law and state observer is used together in a separation principle, the stability of the complete feedback loop must be considered. Stability follows in our case directly from [23, Appendix C] as the UGES control law and the UGES state observer are cascaded.

V. DP IN ICE CASE STUDY

When marine vessels interact with high concentrations of sea-ice (above 6/10th surface coverage), the dynamics are substantially different from open water conditions, and conventional open water DP systems are known to be insufficient [3], [18], [25]–[27]. However, full-scale, model-scale, and numerical experiments have demonstrated that high-uptime positioning is possible given feasible ice conditions and a reactive DP system [26], [28]–[31]. The first is ensured by an icebreaker support fleet that breaks up the incoming natural ice cover and creates a channel of small ice floes for the protected DP vessel to operate in. A reactive DP system can be synthesized by removing the wave filtering and retuning the control system more aggressively [5]. However, since this is based on a simplified open water model lacking the complex and rapidly varying ice dynamics, it will struggle to track and counteract the external loads as these increase. In [32] and [33] this problem is alleviated by assuming an accurate ice load measurement. However, practical and reliable measurement systems are not available today. Neither are sufficiently accurate control models capturing the ice dynamics [27], [34]. One reason for this is that the ice loads depend on the complex in-situ state and properties of the ice floes in direct and indirect contact with the vessel. As the presented AFF methodology avoids the ice load specific measurement and modelling challenges, it is seen as a candidate solution for a reactive system.

A. PRELIMINARIES

This study is divided into two cases. The first investigates a dataset from a model scale experiment performed at the Hamburg Ship Model Basin (HSVA) as a part of the European research and development project DYnamic Positioning in ICe (DYPIC). Project overviews can be can be found in [35] and [36]. The second case is a closed-loop numerical simulation using a state-of-the-art high-fidelity numerical program.

For both cases the conceptual and experimentally tested Arctic drillship (ADS) is considered. This was one of

FIGURE 7. The model scale Arctic Drillship during experimental testing at HSVA. Courtesy of DYPIC.

TABLE 2. The ADS main particulars. FS denotes full scale, MS model scale.

Parameter	FS	MS
Length in design waterline (m)	197.73	6.67
Length between perp. (m)	184	6.13
Breath, moudled (m)	41.33	1.37
Draught at design waterline (m)	12	0.4
Stem angle at design waterline (°)	45	45
Frame angle at midship (°)	45	45
Displacement volume (m^3)	68457	2.535
Centre of gravity from aft. p. (m)	95.34	3.18
Block coefficient	0.75	0.75
Metacentric height (m)	10.71	0.357
Total thrust (N)	$7.2{\cdot}10^6$	270

TABLE 3. The ADS azimuth thruster arrangement.

No.	Comment	x [mm]	y [mm]	F_{max} [N]
1	Port-Bow	2272	316	45
2	Center-Bow	2644	0	45
3	Stb-Bow	2272	-316	45
4	Center-Stern	-3102	0	45
5	Port-Stern	-2664	190	45
6	Stb-Stern	-2664	-190	45

two vessels tested during DYPIC, and it is seen in Figure 7. Its main particulars and azimuth thruster arrangement are found in Tables 2 and 3. In the model ice basin at HSVA the position and orientation of the vessel was measured using a Qualisys position reference system. The linear accelerations and rotation rates were measured using an onboard IMU, and the actuation output was measured by load cells in each thruster. All data were logged with 50 Hz. Further description of the ADS is found in [27].

B. CASE 1: OPEN-LOOP DISTURBANCE ESTIMATION

Model scale trials in ice basins are often used since full scale trials are both impracticality and expensive as it is performed in an uncontrollable environment [3], [37], [38]. The foundation for this part of the case study is the free floating DP experiment 5200 dataset. This was a free floating

TABLE 4. DYPIC experiment 5200 ice field properties.

Property	Value
Ice concentration	70 %
Ice thickness	0.025 m
Min floe size	0.5 x 0.5 m
Max floe size	1.5 x 1.5 m
Ice drift velocity	0.047 m/s

TABLE 5. DYPIC experiment 5200 DP setpoint segmentation.

No.	Setp. (x [m] ,y [m],ψ [deg])	Length [m]
1.	0, 0, 0°	17
2.	0, 0, 5°	17
3.	0, 0, 10°	17

DP test where the vessel tracked a reference frame moving with constant velocity through the basin. A commercial ice-adapted DP system controlled the vessel. As the vessel progressed in the basin, the heading setpoint was altered to obtain an oblique angle with respect to the ice drift. It should also be mentioned that the vessel maintained position and heading within allowed tolerances, for all setpoints. However, the ice conditions were relatively mild and the ice concentration then allows the ice floes to be pushed away, rather than broken or rafted by the advancing ship. Key experimental parameters are given in Tables 4 and 5. For a more in-depth treatment of the experimental setup, see [27].

As the ADS IMU only contained one accelerometer, the rotational components of the acceleration vector could not be determined. However, the short IMU lever arm together with an experimental setup catering for low rotational rates enables to assume that the measured linear accelerations are close to the ones at CO. Thus, a Kalman filter applying a subset of the model (30a)-(30d) was implemented. To get an idea of the angular acceleration a differentiation of the IMU gyro measurement was performed.

The load estimation was performed using the following filter, derived from (58a) by employing the τ actuation signal and assuming $\rho(\eta, \nu) = 0$,

$$\dot{\Delta} = \mu(Ma(t) - \tau_o - \Delta) \tag{68}$$

where $\Delta \in \mathbb{R}^3$ is the disturbance estimate, and $\tau_o \in \mathbb{R}^3$ is the measured actuation vector. For this case study $\mu = 1$ was used.

Figure 8 shows the recorded position and heading of the vessel in the moving reference frame and the planar loads found by the open-loop disturbance estimation compared to the actuation output. It can be seen that the estimates correspond well with the actuation level, but are not identical. This may be attributed to the fact that the vessel experienced perturbations which were not effectively handled by the control system, causing minor deviation from the setpoint (as seen in the position and heading data). These are especially evident towards the end of the experiment in y. Interestingly, the AFF load estimates seem to capture the disturbances. The physical explanation for the increase in

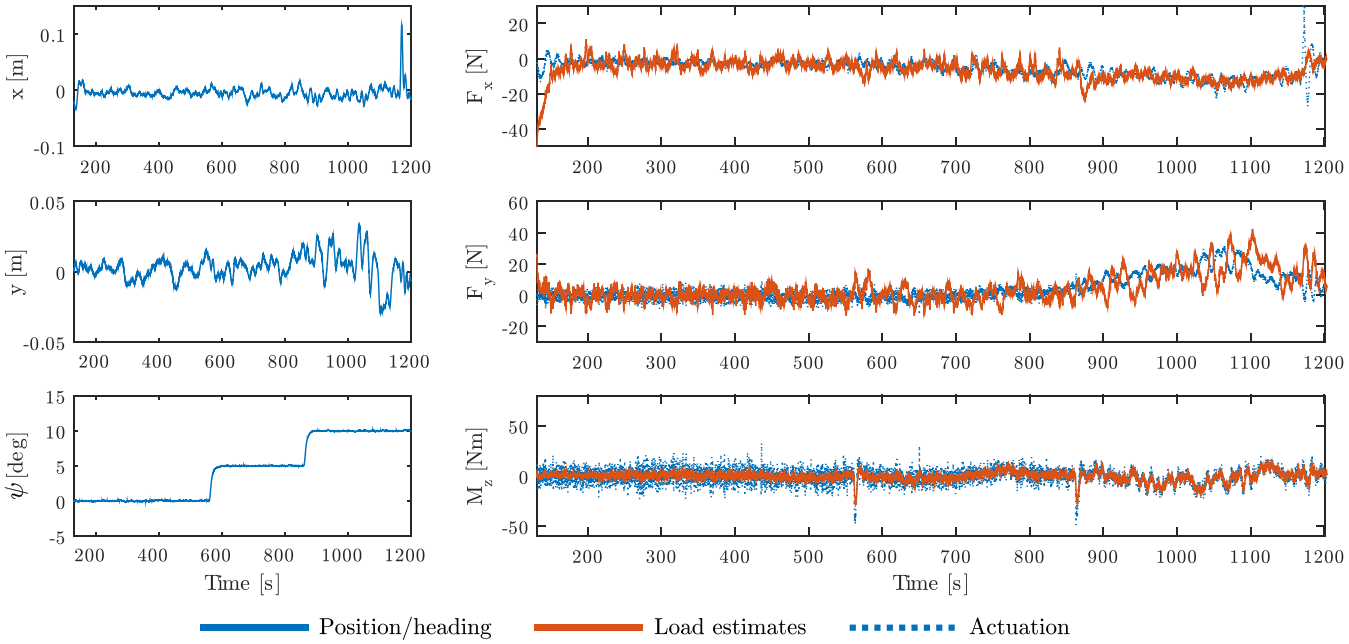

FIGURE 8. Left: the recorded position and heading of DYPIC experiment 5200 with respect to the moving reference frame. Right: the body frame open-loop disturbance estimates compared to the vessel actuation (in opposite sign for eased interpretation). All data in model scale.

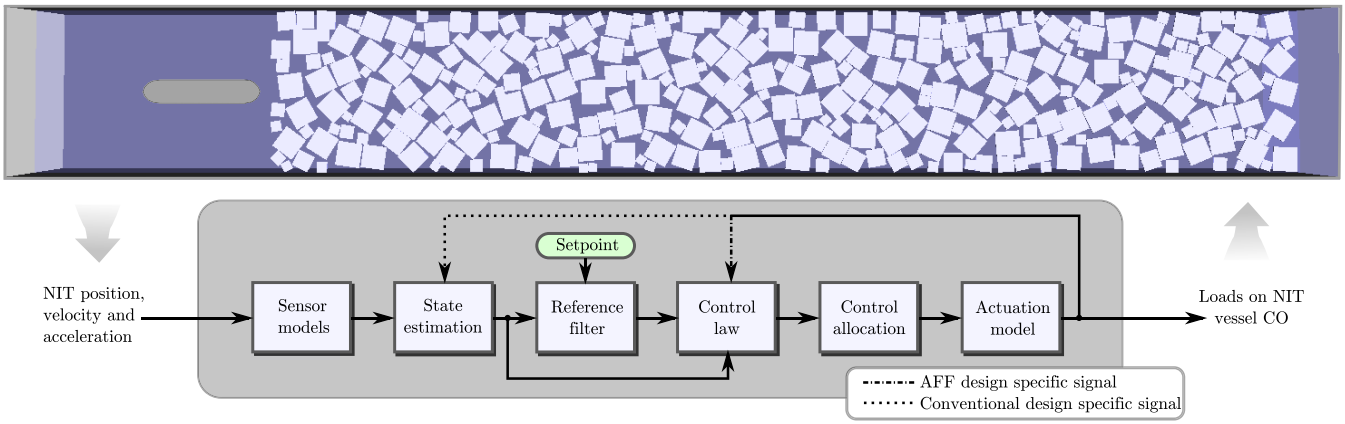

FIGURE 9. Illustration featuring a rendering from the numerical ice tank indicating the experimental setup, and the overall topology of the simulation program.

load and variation is compaction of the ice cover as the vessel advances towards the end of the basin.

The results indicates that the methodology is able to estimate the dynamic acceleration from an accelerometer with the previously mentioned challenges, and calculate the external load including rapidly varying dynamics. However, no definitive verification of the method is possible with this dataset as no independent measurement system was used.

C. CASE 2: CLOSED-LOOP SIMULATION

This study uses the DP in ice development framework featured in [5]. It closes the loop between a control system and the numerical model of [39], which hereafter will be referred to as the Numerical Ice Tank (NIT). Figure 9 provides an overview. As the aforementioned references treat both the setup in-depth, only a brief summary is given together with the case setup.

The NIT computes the vessel's dynamics in 6 DOF without wind and waves using a physics engine with tailored routines for ice material modelling. Each simulation is comprised of the following five interconnected elements: the vessel, the towing carriage, the ice floes, the water volume, and the ice tank boundaries. The vessel is simulated as a rigid body in 6 DOF without deformations. The towing carriage is not used in this paper as only free-floating DP mode is considered. The ice floes are simulated as breakable bodies with uniform thickness in 6 DOF. The initial ice floe sizes and floe positions are generated by an ice field generation algorithm that aims to

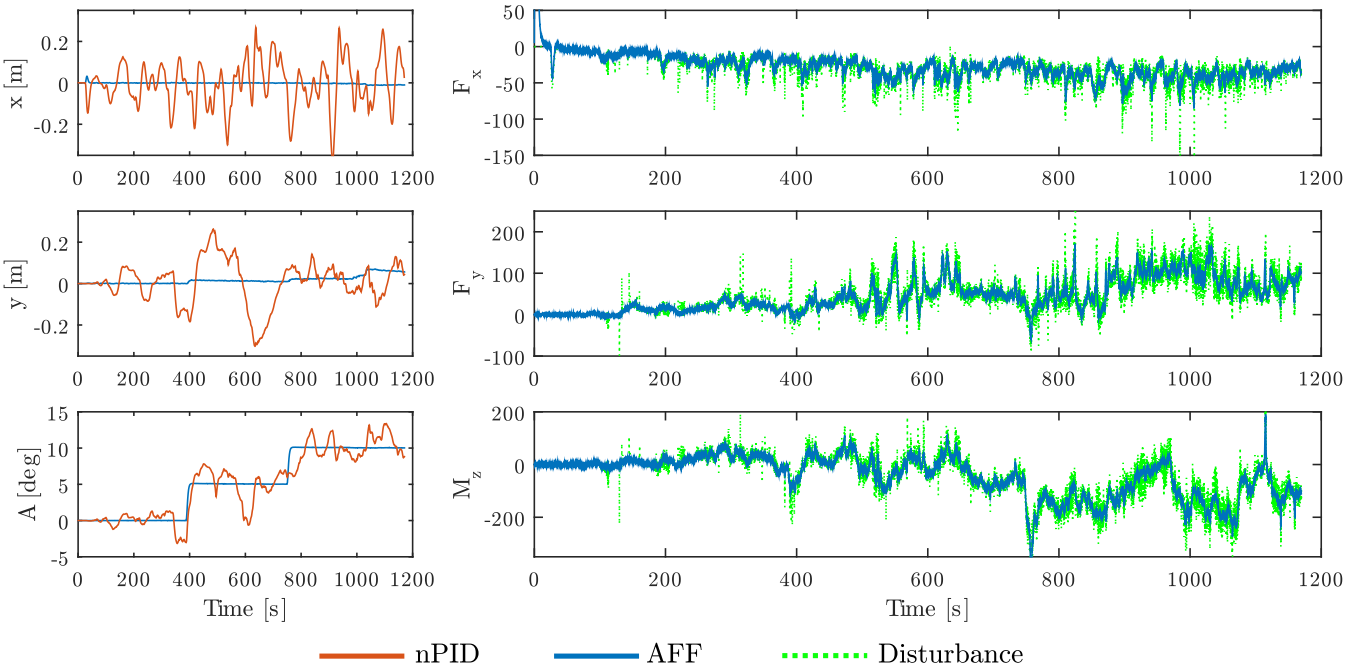

FIGURE 10. Left: Comparison between ice-adapted nPID and the proposed AFF controller. Right: The estimated disturbance by the rejection filter compared to the simulated disturbance.

produce a specified ice field. The water is simulated as a static plane that produces buoyancy and drag loads on the vessel and the ice floes.

The motion variables of the vessel in NIT are defined in three reference frames: the tank-fixed frame {t} which is non-rotational and fixed to the stationary tank boundaries; the body frame {b} which is fixed to the vessel; and the ice floe frames {i} which are fixed to each individual ice floe. For DP, a fourth reference frame, the positioning frame {n}, is introduced. This is non-rotational and follows a pre-defined trajectory to simulate ice drift in the stationary ice cover. For DP development, {n} is considered inertial, and in this study the DP vessel will be set to track a fixed setpoint in this frame. This approximation is common for simulating ice drift in ice tank testing [36].

The sensor models simulate onboard equipment for measuring the motions of the vessel. They are implemented by first transforming the NIT vessel motion output (i.e. position, orientation, linear velocity, and angular rate) from {t} to {n} and {b}. Then, sensor dynamics and noise are added to the signals. The accelerometers are simulated realistically with both gravity and bias errors. The actuator models implement the dynamics of the thruster system onboard the vessel. This is approximated with first order dynamics as described by [2].

Two control systems are compared, one with AFF using the accelerometer configuration as seen in Table 6, a state observer as described in Section III-C, the control law of Proposition 4.2, and the direct disturbance rejection filter in (68). For comparison, a state-of-the-art nonlinear PID-type (nPID) control law combined with a nonlinear DP observer, both adapted to ice conditions as described in [5]. In practice this is a more aggressively tuned DP controller where the wave filter has been removed. The challenges with such a control system in harsh environments has been covered above. Two simulations are run with identical ice covers. One for each control system.

TABLE 6. Placement of accelerometers in the ADS relative to CO for the numerical simulation.

ACC nr.	X [m]	Y [m]	Z [m]	Note
1	3	0	0.3	Bow
2	0	0.6	0	Starboard
3	-3	0	0.3	Stern
4	0	-0.6	0	Port

TABLE 7. Numerical simulation ice conditions.

Parameters	Value	Unit
Water density	1000	kg/m^3
Ice density	900	kg/m^3
Ice flexural strength	45.9	kPa
Ice compressive strength	92	kPa
Ice elastic modulus	10	Mpa
Ice concentration	85	%
Ice thickness	40	mm
Ice drift velocity	0.047	m/s
Max. floe size	1.5	m
Min. floe size	0.5	m

The control objective of the scenario is identical to that of experiment 5200. However, the ice concentration is more severe which constitute a significantly more challenging operational environment than in the model scale experiment. A summary of the ice parameters used are found in Table 7.

The simulation results are shown in Figure 10 where the left column present the position and heading accuracy. This shows that the positioning capabilities of AFF system outperforms the nPID. The right column of Figure 10 presents the disturbance estimation accuracy of the AFF system. It shows that it is able to track and filter the external load well.

VI. CONCLUSIONS

This paper presented a control system design that uses acceleration measurements for rigid body marine motion control subject to harsh environments. The challenges of obtaining a full state measure of the dynamic acceleration was addressed with a setup of four accelerometers placed in a specific configuration that serves as input to the state observer. The main contribution of the paper is the novel method for integrating the dynamic acceleration as an acceleration feedforward in the control law. The proposed design was investigated with both experimental data and high-fidelity simulations, both showing feasibility and effectiveness of the proposed control setup.

REFERENCES

[1] T. I. Fossen, *Handbook of Marine Craft Hydrodynamics and Motion Control*. New York, NY, USA: Wiley, 2011.

[2] A. J. Sørensen, "Marine control systems propulsion and motion control of ships and ocean structures lecture notes," Dept. Marine Technol., Norwegian Univ. Sci. Technol., Trondheim, Norway, Tech. Rep. UK-12-76, 2012.

[3] N. A. Jenssen, S. Muddesitti, D. Phillips, and K. Backstrom, "DP in ice conditions," in *Proc. Dyn. Positioning Conf.*, Houston, TX, USA, 2009.

[4] D. Bray, *The DP Operator's Handbook*. London, U.K.: The Nautical Institute, 2011.

[5] Ø. K. Kjerstad and R. Skjetne, "Modeling and control for dynamic positioned marine vessels in drifting managed sea ice," *Model., Identificat. Control*, vol. 35, no. 4, pp. 249–262, 2014.

[6] R. Skjetne, L. Imsland, and S. Løset, "The arctic DP research project: Effective stationkeeping in ice," *Model., Identificat. Control*, vol. 35, no. 4, pp. 191–210, 2014.

[7] *Guidelines for Vessels With Dynamic Positioning Systems*, Int. Maritime Org., London, U.K., Jun. 1994.

[8] D. Titterton and J. Weston, *Strapdown Inertial Navigation Technology* (Progress Astronautics Aeronautics), 2nd ed. Washington, DC, USA: AIAA, 2005.

[9] K.-P. Lindegaard, "Acceleration feedback in dynamic positioning," Ph.D. dissertation, Dept. Eng. Cybern., Norwegian Univ. Sci. Technol., Trondheim, Norway, 2003.

[10] Ø. K. Kjerstad, R. Skjetne, and N. A. Jenssen, "Disturbance rejection by acceleration feedforward: Application to dynamic positioning," in *Proc. IFAC World Congr.*, Milan, Italy, 2011, pp. 2523–2528.

[11] Ø. K. Kjerstad and R. Skjetne, "Observer design with disturbance rejection by acceleration feedforward," in *Proc. ROCOND*, Aalborg, Denmark, 2012, pp. 535–540.

[12] P. Batista, C. Silvestre, and P. Oliveira, "On the observability of linear motion quantities in navigation systems," *Syst. Control Lett.*, vol. 60, no. 2, pp. 101–110, Feb. 2011.

[13] A. Buhmann, C. Peters, M. Cornils, and Y. Manoli, "A GPS aided full linear accelerometer based gyroscope-free navigation system," in *Proc. IEEE/ION Position, Location, Navigat. Symp.*, Apr. 2006, pp. 622–629.

[14] C.-W. Tan and S. Park, "Design of accelerometer-based inertial navigation systems," *IEEE Trans. Instrum. Meas.*, vol. 54, no. 6, pp. 2520–2530, Dec. 2005.

[15] B. Zappa, G. Legnani, A. van den Bogert, and R. Adamini, "On the number and placement of accelerometers for angular velocity and acceleration determination," *Trans. ASME*, vol. 123, no. 3, pp. 552–554, Mar. 2001.

[16] *MRU 5+—The Ultimate Marine Motion Sensor*, Kongsberg Maritime AS, Kongsberg, Norway, 2014.

[17] A. S. P. Maritime, "R/V Gunnerus summary report," Parker Maritime AS, Stavanger, Norway, Tech. Rep. 1006007-10000128, 2013.

[18] S. Kerkeni, X. Dal Santo, and I. Metrikin, "Dynamic positioning in ice—Comparison of control laws in open water and ice," in *Proc. 32nd Int. Conf. Ocean, Offshore Arctic Eng.*, 2013.

[19] R. E. Kalman and R. S. Bucy, "New results in linear filtering and prediction theory," *Trans. ASME. D, J. Basic Eng.*, vol. 83, no. 1, pp. 95–107, Mar. 1961.

[20] J.-P. Gauthier and I. Kupka, *Deterministic Observation Theory and Applications*. Cambridge, U.K.: Cambridge Univ. Press, 2001.

[21] G. Besançon, "Observer design for nonlinear systems," in *Advanced Topics in Control Systems Theory* (Lecture Notes in Control and Information Science). Springer, 2006.

[22] P. Batista, C. Silvestre, P. Oliveira, and B. Cardeira, "Accelerometer calibration and dynamic bias and gravity estimation: Analysis, design, and experimental evaluation," *IEEE Trans. Control Syst. Technol.*, vol. 19, no. 5, pp. 1128–1137, Sep. 2011.

[23] H. K. Khalil, *Nonlinear Control*. Upper Saddle River, NJ, USA: Pearson Education Ltd., 2015.

[24] M. Arcak and P. Kokotović, "Redesign of backstepping for robustness against unmodelled dynamics," *Int. J. Robust Nonlinear Control*, vol. 11, no. 7, pp. 633–643, Jun. 2001.

[25] A. Gürtner, B. H. H. Baardson, G.-O. Kaasa, and E. Lundin, "Aspects of importance related to arctic DP operations," in *Proc. ASME 31st Int. Conf. Ocean, Offshore Arctic Eng. (OMAE)*, Rio de Janeiro, Brazil, Jul. 2012, pp. 617–623.

[26] T. Hals and N. A. Jenssen, "DP ice model test of arctic drillship and polar research vessel," in *Proc. ASME 31st Int. Conf. Ocean, Offshore Arctic Eng. (OMAE)*, Rio de Janeiro, Brazil, Jul. 2012, pp. 467–472.

[27] O. Kjerstad, I. Metrikin, S. Løset, and R. Skjetne, "Experimental and phenomenological investigation of dynamic positioning in managed ice," *Cold Regions Sci. Technol.*, vol. 111, pp. 67–79, Mar. 2015.

[28] A. Keinonen and E. H. Martin, "Modern day pioneering and its safety in the floating ice offshore," in *Proc. Int. Conf. Exhibit. Perform. Ships Struct. Ice*, vol. 1. 2012, pp. 1–11.

[29] P. P. Liferov, "Station-keeping in ice—Normative requirements and informative solutions," in *Proc. Arctic Technol. Conf.*, Houston, TX, USA, 2014, pp. 1–12.

[30] I. Metrikin, S. Løset, N. A. Jenssen, and S. Kerkeni, "Numerical simulation of dynamic positioning in ice," *Marine Technol. Soc. J.*, vol. 47, no. 2, pp. 14–30, Mar./Apr. 2013.

[31] Å. Rohlén, "Relationship between ice-management and station keeping in ice," in *Proc. Presentation Dyn. Positioning Conf.*, Houston, TX, USA, 2009.

[32] D. T. Nguyen, A. H. Sørbø, and A. J. Sørensen, "Modelling and control for dynamic positioned vessels in level ice," in *Proc. Conf. Manoeuvring Control Marine Craft*, 2009, pp. 229–236.

[33] D. H. Nguyen, D. T. Nguyen, S. T. Quek, and A. J. Sørensen, "Position-moored drilling vessel in level ice by control of riser end angles," *Cold Regions Sci. Technol.*, vol. 66, nos. 2–3, pp. 65–74, May 2011.

[34] K. J. Eik, "Ice management in arctic offshore operations and field developments," Ph.D. dissertation, Dept. Civil Transport Eng., Norwegian Univ. Sci. Technol., Trondheim, Norway, 2010.

[35] N. A. Jenssen *et al.*, "DYPIC—A multi-national R&D project on DP technology in ice," in *Proc. Dyn. Positioning Conf.*, Houston, TX, USA, 2012.

[36] A. Haase and P. Jochmann, "Different ways of modeling ice drift scenarios in basin tests," in *Proc. ASME 32nd Int. Conf. Ocean, Offshore Arctic Eng.*, Nantes, France, Jun. 2013, pp. 1–9.

[37] D. Deter, W. Doelling, L. Lembke-Jene, and A. Wegener, "Stationkeeping in solid drift ice," in *Proc. Dyn. Positioning Conf.*, Houston, TX, USA, 2009.

[38] W. L. Kuehnlein, "Philosophies for dynamic positioning in ice-covered waters," in *Proc. Offshore Technol. Conf.*, Houston, TX, USA, 2009, pp. 1–7.

[39] I. Metrikin, "A software framework for simulating stationkeeping of a vessel in discontinuous ice," *Model., Identificat. Control*, vol. 35, no. 4, pp. 211–248, 2014.

ØIVIND KÅRE KJERSTAD was born in Norway in 1985, and started his career as a Factory Worker with the maritime industry in Western Norway in 2001. In 2005, after receiving the skilled craftsmanship diploma, he began studying cybernetics with the Norwegian University of Science and Technology. He received the M.Sc. degree in 2010. He joined the research project KMB Arctic DP to pursue the Ph.D. During this, he has participated in research cruises to Svalbard and East Greenland, and model scale experiments in ice. His research interests are within marine motion control systems and arctic technology.

ROGER SKJETNE received the M.Sc. degree in control engineering from the University of California at Santa Barbara, in 2000, and the Ph.D. degree from the Norwegian University of Science and Technology (NTNU), in 2005, for which the thesis was awarded the Exxon Mobil prize for best Ph.D. thesis in applied research. Prior to his studies, he was an Electrician with Aker Elektro AS on numerous oil installations for the North Sea. From 2004 to 2009, he was with Marine Cybernetics AS, working on hardware-in-the-loop simulation for testing safety-critical marine control systems. Since 2009, he has been the Professor of Marine Control Engineering with the Department of Marine Technology, NTNU, where he is currently the Leader of the Research Group on Marine Structures. His research interests are within arctic station keeping operations and ice management systems for ships and rigs, environmentally robust control of shipboard electric power systems, and nonlinear control theory for motion control of single and groups of marine vessels. He managed for the KMB Arctic DP research project, and is a Leader of the ice management work package in the CRI Sustainable Arctic Marine and Coastal Technology, and is an Associate Researcher with the CoE Centre for Ships and Ocean Structures and CoE Autonomous Marine Operations and Systems.